J Mol Model (2015) 21: 316
DOI 10.1007/s00894-015-2856-1

ORIGINAL PAPER

Systematic analysis of structural and spectroscopic properties of neptunimine ($HN=NpH_2$) and plutonimine ($HN=PuH_2$)

Peng Li[1] · **Wenxia Niu**[2] · **Tao Gao**[3]

Received: 13 September 2015 / Accepted: 2 November 2015 / Published online: 25 November 2015

Abstract The structures, stabilities, nature of bonding, and spectroscopic properties of the new actinide imine molecules, neptunimine ($HN=NpH_2$) and plutonimine ($HN=PuH_2$), in the gas phase have been systematically explored at different levels of theory. Our calculation indicates that $HN=AnH_2$ (An=Np, Pu) should be nonplanar and have a quartet ($\tilde{X}^4A$) and quintet ($\tilde{X}^5A$) ground state, respectively. The nature of the chemical bonding in these molecules were investigated by employing topological methods including electron localization function (ELF), atoms in molecules (AIM) as well as natural bond orbital analysis (NBO). The results showed that these actinide complexes possess relatively strong An=N multiple bonds between the An *6d-5f* hybrid orbitals with N *2s-2p* orbitals. The charge decomposition analysis (CDA) diagram demonstrated that the transition of electrons mainly happened inside the AnH_2 of $HN=AnH_2$. Total and partial density of state (TDOS and PDOS) and also overlap population density of state (OPDOS) diagrams analysis were implemented. The IR and Raman spectra were theoretically simulated as a convenient way to confirm the existence of the actinide imine complexes in further experiments.

✉ Wenxia Niu
nwx_ky@163.com

Peng Li
lip@sxu.edu.cn

[1] College of Physics and Electronic Engineering, Shanxi University, Taiyuan 030006, China

[2] Department of Physics, Taiyuan Normal University, Taiyuan 030031, China

[3] Institute of Atomic and Molecular Physics, Sichuan University, Chengdu 610065, China

Keywords IR and Raman spectra · Multiple bonds · Neptunimine · Plutonimine · Structures · Topological analysis

Introduction

The nature of the multiple bonding between actinide (An) and main-group ligands (L) is of considerable research importance, due to interest in the behavior of *5f* electrons [1–16]. A thorough understanding of An-L molecular structures could be helpful to ameliorating nuclear waste clean-up or devising new nuclear waste repositories. In addition to the well-known U≡O triple bonds in the uranyl ion, the U=O and U=NR multiple bonds in oxide and imido complexes are well established and understood classes of An-L multiple bonds [17].

It is found that the lone pair electrons of N atom in NH_3 plays a vital role in the bonding of actinide imine molecules. Recently, laser-ablated Th or U atoms reacted with NH_3 in the gas phase to form thorimine ($HN=ThH_2$) or uranimine ($HN=UH_2$) were detected and characterized by infrared spectroscopic identification in Andrews' laboratories [18, 19]. On the theoretical side, Andrews et al. provided insights into the density functional theory study of thorimine ($HN=ThH_2$) and uranimine ($HN=UH_2$) molecule. Their calcuations showed that the $HN=ThH_2$ and $HN=UH_2$ have the analogous structure, and appreciable N≡Th and N≡U partial triple-bond character which has an important contribution from the *f* orbitals [18]. In our recent work, the reaction mechanism of U + NH_3 in gas phase has been investigated in detail at different levels of theory [20]. Given the greater number of *5f* orbitals available on Np and Pu atom, is the nature of the N-Np or N-Pu bonding in the actinide imine molecules as similar as in $HN=ThH_2$ and $HN=UH_2$?

The main objective of this work is to report the first detailed theoretical evidence of the neptunimine ($HN=NpH_2$) and

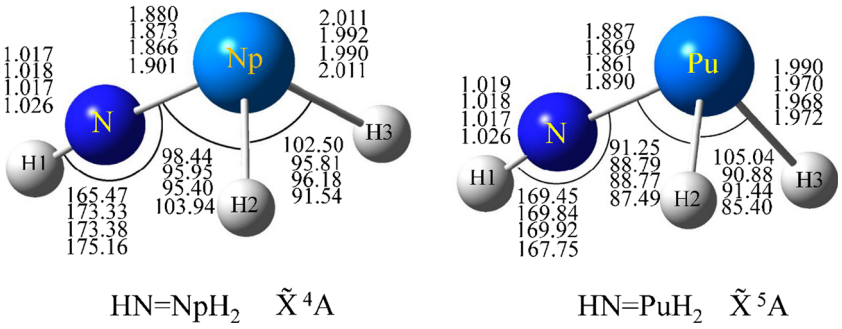

Fig. 1 Structures and geometric parameters of $HN=NpH_2$ and $HN=PuH_2$ molecules optimized at the B3LYP/SDD, B3PW91/SDD, PBE0/SDD, and PW91/SDD levels of theory (from top to bottom rows, respectively). Bond distances are in Å, and angles are in degrees

plutonimine ($HN=PuH_2$) molecules. The bonding characters were investigated in terms of diverse analyses including electron localization function (ELF), atoms in molecules (AIM), and natural bond orbital (NBO). The roles of *5f* orbitals were diagrams analyzed by total density of state (TDOS) and partial density of state (PDOS) together with overlap population density of state (OPDOS).

Computational details

Geometry optimization and frequency calculations of the minima structures were performed at the B3LYP [21, 22], PW91PW91 [23], B3PW91 [24], and PBE0 [25] methods, along with Stuttgart/Bonn relativistic effective core potential (RECP) [26] for Np and Pu atom, the 6-311++G(d,p) basis set for N and H atoms. This small-core RECP, is named SDD, replaces 60 electrons in inner shells, leaving the n≥5 shell as the valence electrons. These calculations were carried out using the Gaussian 03 programs [27]. All of the structures were identified to be local minima without any imaginary frequencies. The present computational method has been successfully carried out in previous actinide systems calculations [28–32], and specifically, B3LYP/SDD and PW91/SDD methods were shown to have good performance in the structure and frequencies investigation for $HN=ThH_2$ and $HN=UH_2$ compounds [18, 19].

A topological description of all species with the aim of deeply understanding the nature of the bonding was performed. The wavefunction files (.wfn) which obtained by using the Gaussian 03 programs were used as input files of the Multiwfn [33] package to perform the ELF [34, 35] and AIM [36] analysis. It is worth mentioning that ELF and AIM are useful means of analyzing molecular interactions and have been successfully applied in many investigations. In order to gathering insights about the participation of *5f* orbitals in the chemical bonds of complexes, TDOS, PDOS, and OPDOS were also calculated [37, 38]. In addition, CDA (charge decomposition analysis) were performed to obtain a deep insight into the nature of the charge transformation [39].

Results and discussion

Geometric structures

Many possible structures of $HN=NpH_2$ and $HN=PuH_2$ were constructed. Different possible spin states were considered. After optimization, the stable conformation in the gas phase was located. The optimized geometries of the $HN=NpH_2$ and $HN=PuH_2$ are shown in Fig. 1, and the optimized geometries show little dependence on the level of theory. The electronic state (ES) and relative energies of the stable structures are listed in Table 1.

Our results indicate that the $HN=NpH_2$ and $HN=PuH_2$ molecules should be nonplanar and have a similar structure as $HN=ThH_2$ and $HN=UH_2$ [18, 19]. The $HN=NpH_2$ molecule forms a stable nonplanar equilibrium structure with Np–N bond distances of 1.880Å, as can be seen from Fig. 1. The ground electronic state of $HN=NpH_2$ molecule is identified as the quartet $\tilde{X}^4A$. On the other hand, the calculation on $HN=PuH_2$ predicted that the molecules have a quintet $\tilde{X}^5A$ ground state. The N-Pu bond lengths were calculated as 1.887 Å. The N-An bonds are slightly shorter than the ones in $HN=ThH_2$ and $HN=UH_2$ (1.951 and 1.903Å at B3LYP/SDD level of theory, respectively).

Table 1 The electronic state and relative energies (in kcal mol^{-1}) for the stable structures $HNNpH_2$ and $HNPuH_2$ molecules

	States	B3LYP	B3PW91	PBE0	PW91
$HNNpH_2$	^2A	7.064	18.970	21.097	13.825
	$\tilde{X}^4A$	0.000	0.000	0.000	0.000
	^6A	18.848	31.817	30.909	28.720
	^8A	76.774	89.551	88.544	88.502
$HNPuH_2$	^3A	28.411	26.602	27.390	25.094
	$\tilde{X}^5A$	0.000	0.000	0.000	0.000
	^7A	23.608	18.487	17.059	22.085
	^9A	69.769	68.354	68.613	71.137

All calculations used the SDD for Np (Pu) and 6-311++G(d,p) for H and N atoms

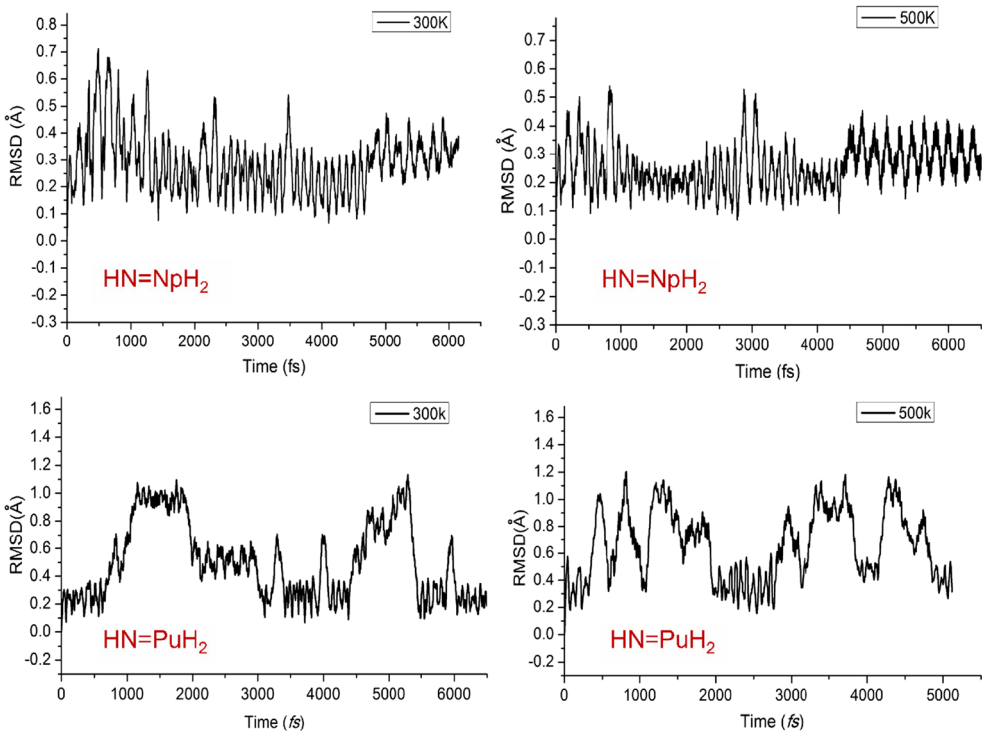

Fig. 2 The RMSD through time at different temperatures for the $HN{=}NpH_2$ and $HN{=}PuH_2$ molecules

For the system which does not have the experimental values about the structure parameters, we should routinely do our calculations with different functional and see if they give consistent results [40]. Our calculations contain pure GGA functional and hybrid density functional with small core relativistic effective potentials (RECP) and should give reliable results on geometries and energies of the $HN{=}NpH_2$ and $HN{=}PuH_2$ molecules. As shown by the relative energies of the stable structures listed in Table 1, the relative energies are consistent at various levels of theory. The only incongruity is that B3LYP/SDD underestimated the relative energies of $HN{=}NpH_2$.

The ab initio MD simulations at 300 and 500 K, respectively, are performed at B3PW91 level of theory to further confirm the stability of the $HN{=}NpH_2$ and $HN{=}PuH_2$ structure. Both simulations are carried out for 5 ps using a BOMD [41] implemented in the Gaussian 03 program. The root mean square displacement (RMSD) of MD trajectory at different temperatures is depicted in Fig. 2. Within the time frame of our simulations, RMSD results indicate that $HN{=}NpH_2$ icosahedral structure keeps its identity at both room temperature (300 K) and high temperature (500 K). However, one can see that the thermal distortions of $HN{=}PuH_2$ have large fluctuations than that of $HN{=}NpH_2$, which reveals that the $HN{=}NpH_2$ is more stable than $HN{=}PuH_2$.

IR and Raman spectroscopy

The harmonic vibrational frequencies of the ground state $HN{=}NpH_2$ and $HN{=}PuH_2$ structure were calculated at the B3PW91 and PBE0 levels of theory as the geometry optimization. The results are collected in Table 2. Predicted IR spectra in the gas phase are depicted in Fig. 3. The strongest IR

Table 2 Comparison of calculated harmonic frequencies for the $HNNpH_2$ and $HNPuH_2$

	B3LYP	B3PW91	PBE0	PW91	Mode
$HNNpH_2$	3554.7	3544.6	3569.3	3425.4	N-H stretch
	1467.8	1540.1	1544.5	1617.7	NpH_2 stretch
	1387.1	1493.8	1496.1	1423.2	NpH_2 stretch
	817.1	845.4	860.3	782.9	N-Np stretch
	532.9	539.4	549.1	560.9	H-N-Np bend
	516.0	505.4	510.8	502.3	H-N- Np bend
	384.1	463.1	459.9	439.4	NpH_2 bend
	347.0	317.0	328.3	238.5	NpH_2 bend
	217.9	223.1	213.9	167.2	$NNpH_2$ deform
$HNPuH_2$	3521.1	3538.7	3562.5	3430.9	N-H stretch
	1499.4	1633.8	1624.7	1473.3	PuH_2 stretch
	1455.9	1518.1	1527.4	1382.8	PuH_2 stretch
	760.6	781.3	800.7	737.1	N-Pu stretch
	561.5	538.0	547.5	499.3	H-N-Pu bend
	522.4	523.2	533.1	479.5	H-N-Pu bend
	504.4	432.9	433.1	460.0	PuH_2 bend
	405.6	387.3	397.5	351.4	PuH_2 bend
	371.3	368.5	371.7	304.3	$NPuH_2$ deform

All calculations used the SDD for Np (Pu) and 6-311++G(d,p) for H and N atoms. All frequencies are in cm^{-1}

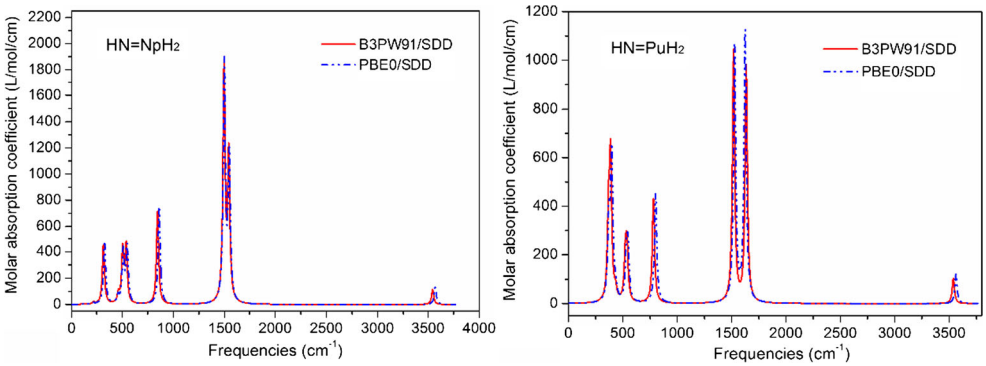

Fig. 3 Simulated IR spectra of $HN{=}NpH_2$ and $HN{=}PuH_2$ molecules

absorption for the $HN{=}NpH_2$ molecule corresponds to the two Np-H stretching modes calculated at 1540.1 and 1493.8 (B3PW91) or 1544.5 and 1496.1 cm^{-1} (PBE0). Similarly to $HN{=}NpH_2$, the strongest IR absorption for the $HN{=}PuH_2$ molecule is the two Pu-H stretching modes. The frequencies 3554.7 cm^{-1} in the $HN{=}NpH_2$ and 3521.1 cm^{-1} in $HN{=}PuH_2$ are caused by N-H stretching vibrations. The Np=N stretching frequency calculated at 845.4 (B3PW91) or 860.3 cm^{-1} (PBE0), is higher than the Pu=N stretching frequency calculated at 781.3 (B3PW91) or 800.7 cm^{-1} (PBE0).

Comparison between the vibrational frequencies of $HN{=}NpH_2$, $HN{=}PuH_2$, $HN{=}ThH_2$, and $HN{=}UH_2$ shows that vibrational modes are similar. This is because they have a similar structure. Taking the strongest IR absorption and N-H stretching as an example, the strongest IR absorption in all these cases are the two An-H stretching modes, and the frequency of N-H stretching vibrations are consistent. Predicted Raman spectra in the gas phase are depicted in Fig. 4. The result shows weak peaks in low frequencies and strong peaks in high frequencies.

Bonding characteristics and orbital interactions

Bonding characteristics

The bonding properties of all of the species involved in this study have been investigated using two different topological methodologies (AIM, ELF) as well as using the natural bond orbital analysis.

The atoms in molecules (AIM) analysis is a powerful tool for the characterization of chemical bonds, and has been successfully utilized to explore the natures of chemical bonding in actinium-complexes [42, 43]. The AIM analyses were performed with wave functions obtained at the B3PW91/SDD level of theory. The topological properties of the (3,-1) bond critical points (bcp) were obtained in terms of the electron density $\rho(r)$ and its Laplacian $\nabla^2\rho(r)$ at the critical bond, the total electron energy density H(r), the potential energy density V(r), and the kinetic electron energy density G(r). Higher V(r) value indicates the electrons are more localized in this regions, whereas large G(r) values correspond to regions where the electrons move faster [44]. The relationships between these parameters are shown in the following equations:

$$\nabla^2\rho(r) = 2G(r) + V(r) \quad (1)$$

$$H(r) = G(r) + V(r). \quad (2)$$

As the traditional topological criterion, a negative $\nabla^2\rho(r)$ corresponds to the covalent bonds. However, this criterion has been proved to be not sufficiently appropriate to describe the bond natures of heavy atoms [45, 46]. Cremer and Kraka [47] proposed that using H(r) as a criterion: for covalent interactions, $|V(r)| > G(r)$, H(r) is negative; whereas closed-shell

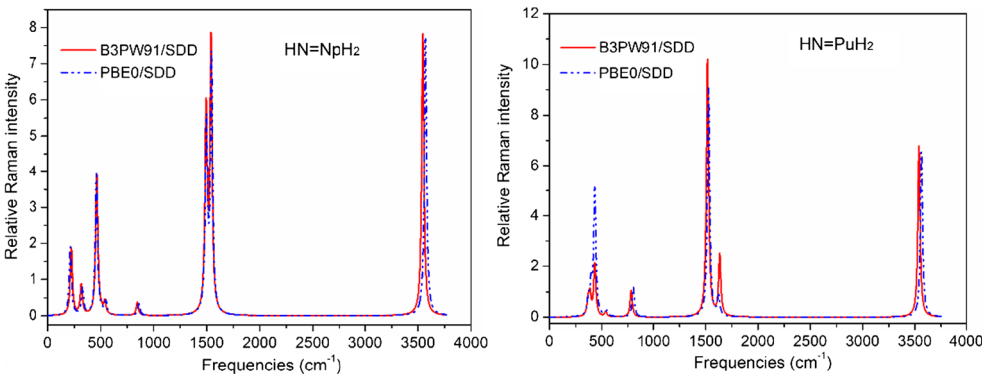

Fig. 4 Simulated Raman spectra of $HN{=}NpH_2$ and $HN{=}PuH_2$ molecules

Table 3 Topological properties of the charge density calculated at the (3,-1) bond critical points for $HNNpH_2$ and $HNPuH_2$ molecules at B3PW91/SDD level of theory

	Species	ρ(r)	$\nabla^2\rho$(r)	G(r)	V(r)	H(r)
HN=ThH_2	Th-H2	0.0827	0.0213	0.0355	−0.0656	−0.0301
	Th-H3	0.0827	0.0213	0.0355	−0.0656	−0.0301
	Th-N	0.1874	0.3852	0.2175	−0.3387	−0.1212
	N-H1	0.3244	−1.4573	0.0579	−0.4802	−0.4223
HN=UH_2	U-H2	0.0901	0.0225	0.0403	−0.0749	−0.0346
	U-H3	0.0901	0.0225	0.0403	−0.0749	−0.0346
	U-N	0.2099	0.4424	0.2549	−0.3992	−0.1443
	N-H1	0.3236	−1.4614	0.0567	−0.4789	−0.4222
HN=NpH_2	Np-H2	0.0967	0.0101	0.0423	−0.0822	−0.0399
	Np-H3	0.0967	0.0101	0.0423	−0.0822	−0.0399
	Np-N	0.2227	0.5063	0.2817	−0.4368	−0.1551
	N-H1	0.3243	−1.4621	0.0560	−0.4775	−0.4215
HN=PuH_2	Pu-H2	0.0984	0.0096	0.0434	−0.0845	−0.0411
	Pu-H3	0.0983	0.0097	0.0434	−0.0843	−0.0409
	Pu-N	0.2193	0.5311	0.2810	−0.4293	−0.1483
	N-H1	0.3248	−1.4685	0.0556	−0.4784	−0.4228

All values are in au

interactions, |V(r)| < G(r), H(r) is positive. H(r) was proved to be very adequate to characterize the nature of a bond for a heavy atom system [48, 49].

The AIM parameters calculated at the (3,-1) bcp for HN=NpH_2 and HN=PuH_2 molecules are listed in Table 3. At all BCPs in the HN=NpH_2 and HN=PuH_2 molecules, the H(r) values are negative, the |V(r)|/G(r) ratio exceeds 1.0. All of these quantities mean that the An–H and An–N bonds have covalent character. In order to facilitate comparison of data, we also listed the AIM parameters of HN=ThH_2 and HN=UH_2 at B3PW91/SDD method using the geometric result of the Andrews' study [18, 19]. The results included in Table 3 suggest that the Th–N and U-N bonds also have a covalent character. A lower H(r) value (−0.1551 au) is observed in the Np-N, as compared to H(r) in the Th-N (−0.1212 au), U-N (−0.1443 au), and Pu-N (−0.1483 au) bonds. The $\nabla^2\rho$(r) values of the An-N bonds rise steadily with increasing atomic number (from Th to Pu).

ELF is another useful tool for identifying the bonding characteristics in molecules. It is worth mentioning that the effective core potential (ECP) seems make the ELF calculation fail to provide a clear core-valence separation on the Np and Pu center. However, studies have shown that the deeper actinium core has little impact on the topological properties of valence [29]. The electron density obtained from a small-core ECP calculation is good enough to reproduce not only the correct topology of the actinium-ligand bonds but the values of the local properties as well [43, 49]. Therefore, the small-core RECP we used in this work is probably responsible for these analysis. Figure 5 shows the behavior of two-dimensional (2D) filled-color diagrams of ELF (η=0.70). One can see that there is a disynaptic valence basin between Np and the N atom, which indicates that there is a covalent bond formation between Np and N in complex HN=NpH_2. This conclusion is supported by the AIM analysis, our result shows that there is a (3,-1) BCP between Np and N atom with a relatively low charge density, ρ(r) 0.2227 au, while negative H(r) value (−0.1551) indicates that Np–N bond has a covalent character. This characteristic is also found in the HN=PuH_2. Despite the qualitative similarity there are differences in the Np-H and Pu-H bond. The ELF diagram shows that the combination of Np-H in HN=NpH_2 are more tightened than Pu-H bonds in HN=PuH_2 molecule, this may due to the large atomic covalent radius of Pu (note that *7s* orbital is much more diffuse than *5f*).

Bond dissociation energies (BDE) are a measure of the bond strength in a chemical bond. Firstly, BDE of HN=NpH_2 and HN=PuH_2, calculated by different methods

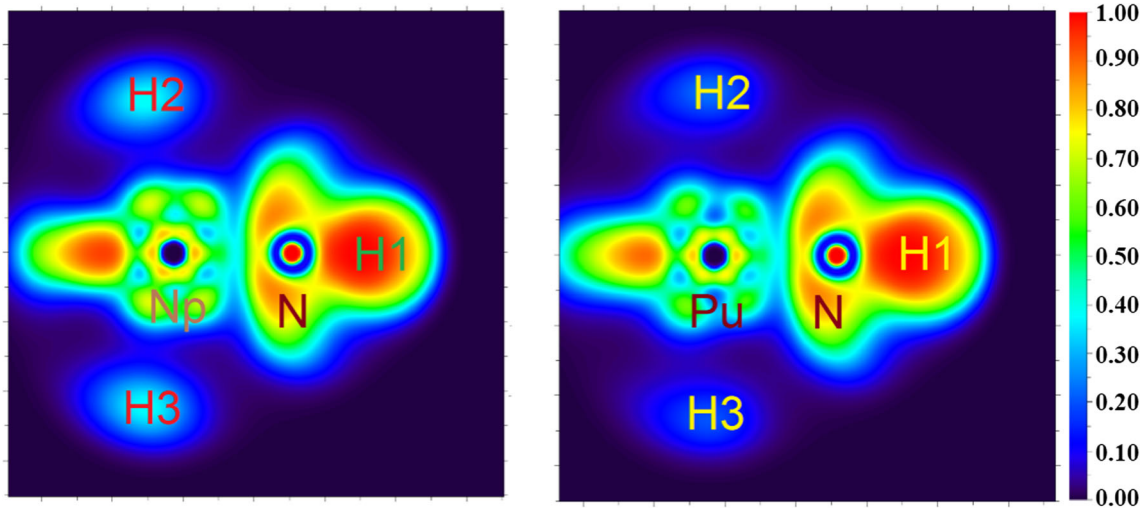

Fig. 5 Two-dimensional (2D) filled-color diagrams of ELF (η=0.70) at the B3PW91/SDD level of theory

as well as the results for $HN{=}ThH_2$ and $HN{=}UH_2$ [19], are collected in Table 4. It can clearly be seen that, as the atomic number increases (from Th to Pu case), the BDE of An-N bond in these complexes decrease. This fact may be due to the delocalization effect of *5f* electrons has steadily diminished from Th to Pu atom. Mayer bond order analysis indicated that An-N bond order are decreased from Th to Pu, the results are reported in Table 5. In these studies, the 6-311++G(d,p) were replaced with 6-311G(d, p) to generate wavefunctions, because the Mayer bond order was not sufficiently appropriate if diffusion functions were used.

With the aim of investigating the nature of An=N bonds, we performed NBO analysis. The results are compared in Table 6. The ionic character (i_{AB}) is also listed in Table 6. The ionic character (i_{AB}) is a good indicator of the chemical bond, indicating the ionicity of the A-B bond, as determined from NBO polarization coefficients c_A, c_B. The i_{AB} is formulated by the following equation [50]:

$$i_{AB} = \left|\left(c_A{}^2 - c_B{}^2\right)/\left(c_A{}^2 + c_B{}^2\right)\right|$$

Where c_A and c_B are the coefficients of natural hybrid orbital.

From the NBO analysis we can conclude that the multiple bonding in $HN{=}AnH_2$ is similar: (1) there are three BD type in N-An; (2) these N-An bond are very polarized, indeed, the An contributions make up only 17.01–21.1 %. Despite these qualitative similarities, there are significant differences. First of all, the N-Th bond in $HN{=}ThH_2$ is a triple bond, and each BD has two electrons. However, in U, Np, and Pu cases, each BD has almost one electron. Secondly, ionic character (i_{AB}) of N-An bond is gradually decreasing from Th, to Np, but have a maximum value in the Pu case. Finally, from Th to Pu, the *5f* orbitals play a more and more important role in An-N bonding.

Table 4 Bond dissociation energies (BDE in kcal mol^{-1}) and An-N bond lengths (r(An-N) in Å) obtained with four different theoretical methods

Compound		B3LYP/SDD	B3PW91/SDD	PBE0/SDD	PW91/SDD
$HN{=}ThH_2$ [a]	*r*(Th-N)	1.951			
	BDE	148.183			
$HN{=}UH_2$ [a]	*r*(U-N)	1.903			1.898
	BDE	125.239			
$HN{=}NpH_2$ [b]	*r*(Np-N)	1.880	1.873	1.866	1.901
	BDE	107.123	123.475	133.867	131.050
$HN{=}PuH_2$ [b]	*r*(Pu-N)	1.887	1.869	1.861	1.890
	BDE	98.877	97.242	97.366	110.571

[a] Reference 19

[b] Our present work

Table 5 Mayer bond order of An-N bond obtained with four different theoretical methods

Molecule	Bond	B3LYP	B3PW91	PBE0	PW91
$HN{=}ThH_2$	N-Th	2.118	2.101	2.095	2.176
$HN{=}UH_2$	N-U	2.118	2.103	2.096	2.180
$HN{=}NpH_2$	N-Np	2.106	2.086	2.097	2.156
$HN{=}PuH_2$	N-Pu	1.986	1.971	1.968	2.033

Orbital interactions

The TDOS, PDOS, and OPDOS were created by convoluting the molecular orbital information with Gaussian curves of unit height and full width at half maximum (FWHM) of 0.05 a.u using Multiwfn. The TDOS, PDOS, and OPDOS curves of $HN{=}NpH_2$ and $HN{=}PuH_2$ at the B3PW91/SDD levels of theory are plotted in Fig. 6. Fragment 1 is defined as Np or Pu atom, fragment 2 is defined as N atom. The vertical dashed line indicates the position of HOMO and LUMO level.

As seen in Fig. 6, the behavior of the DOSs are similar in both $HN{=}NpH_2$ and $HN{=}PuH_2$ cases. At the position of HOMO level, the orbitals of Np (Pu) atom nearly approaches the TDOS line, which means most of the contributions to HOMO came from the Np (Pu) atom orbitals. The PDOS and OPDOS diagrams also show that the Np (Pu) atom and N have bonding characters around −8.16 eV (below the HOMO), as evidenced by the positive OPDOS value. In the region of −21.77 to −9.0 eV, the OPDOS values are negative, indicating in this energy region Np (Pu) and N atom have anti-bonding characters.

In addition to the similarities, the differences are noteworthy. It is readily seen in Fig. 6, the energy gap between HOMO and LUMO of $HN{=}NpH_2$ is larger than that of $HN{=}PuH_2$, indicating the $HN{=}NpH_2$ is more stable than $HN{=}PuH_2$. This fact is also consistent with previous dynamics simulation results. The OPDOS values of $HN{=}PuH_2$ are more negative than that of $HN{=}NpH_2$ in the region of −21.77 to −9.0 eV, suggesting in this energy region the anti-bonding character of Pu=N bond is stronger.

The CDA analyses were performed to obtain a deep insight into the nature of the charge transformation. The results are displayed in Fig. 7, the occupied orbitals are represented by

Table 6 Natural bond orbital analysis for $HN=AnH_2$ (An=Th, U, Np, and Pu) molecules at B3PW91 level of theory

Molecule	q_{An}	q_N	Bond character (An=N)		*i*
$HN=ThH_2$	1.843	−1.339	BD(1) Occ.= 1.993	Th *s*(9.17 %) *p*(0.31 %) *d*(70.77 %) *f*(19.76 %) N *s*(51.78 %) *p*(48.22 %)	0.6598
			BD(2) Occ.= 1.997	Th *s*(4.24 %) *p*(0.66 %) *d*(71.25 %) *f*(23.85 %) N *s*(5.59 %) *p*(94.40 %)	0.6598
			BD(3) Occ.= 1.998	Th *s*(0.00 %) *p*(0.35 %) *d*(75.55 %) *f*(24.10 %) N *s*(0.00 %) *p*(100 %)	0.6066
$HN=UH_2$	1.904	−0.633	BD(1) Occ.= 0.996	U *s*(10.87 %) *p*(0.15 %) *d*(62.15 %) *f*(26.83 %) N *s*(57.60 %) *p*(42.39 %)	0.6201
			BD(2) Occ.= 0.999	U *s*(0.68 %) *p*(0.39 %) *d*(59.45 %) *f*(39.48 %) N *s*(0.005 %) *p*(99.94 %)	0.6027
			BD(3) Occ.= 0.998	U *s*(0.03 %) *p*(0.44 %) *d*(55.65 %) *f*(42.89 %) N *s*(0.00 %) *p*(99.99 %)	0.6291
$HN=NpH_2$	2.368	−0.625	BD(1) Occ.= 0.996	Np *s*(12.36 %) *p*(0.21 %) *d*(58.68 %) *f*(28.74 %) N *s*(57.40 %) *p*(42.59 %)	0.6187
			BD(2) Occ.= 0.998	Np *s*(1.29 %) *p*(0.42 %) *d*(54.30 %) *f*(44.00 %) N *s*(0.82 %) *p*(99.18 %)	0.6201
			BD(3) Occ.= 0.998	Np *s*(0.00 %) *p*(0.15 %) *d*(55.66 %) *f*(44.19 %) N *s*(0.00 %) *p*(99.99 %)	0.5781
$HN=PuH_2$	2.917	−0.678	BD(1) Occ.= 0.994	Pu *s*(11.80 %) *p*(0.36 %) *d*(68.97 %) *f*(18.88 %) N *s*(42.45 %) *p*(57.54 %)	0.6812
			BD(2) Occ.= 0.991	Pu *s*(0.00 %) *p*(0.17 %) *d*(35.60 %) *f*(64.23 %) N *s*(0.00 %) *p*(99.99 %)	0.6777
			BD(3) Occ.= 0.989	Pu *s*(11.31 %) *p*(0.44 %) *d*(37.79 %) *f*(50.46 %) N *s*(17.49 %) *p*(82.50 %)	0.6039

solid lines, and virtual orbitals are represented by dashed lines. The LUMO and HOMO~HOMO-4 of $HN=NpH_2$ and $HN=PuH_2$ were primarily comprised of the corresponding orbitals of NpH_2 and PuH_2, respectively. Therefore, the above electron transitions happened inside NpH_2 and PuH_2. The HOMO and HOMO-1 molecular orbitals for $HN=NpH_2$ and $HN=PuH_2$ were also shown in Fig. 7. These two orbitals correspond most closely to two π bonds found by the NBO analyses.

Conclusions

The structures, stabilities, nature of bonding, and spectroscopic properties of $HN=NpH_2$ and $HN=PuH_2$ were studied using tools derived from the density functional theory. *Ab initio* MD calculations indicated that the $HN=NpH_2$ is more stable than $HN=PuH_2$. Our calculation indicated that both the $HN=NpH_2$ and $HN=PuH_2$ should be nonplanar, and have a quartet ($\tilde{X}^4A$) and quintet ($\tilde{X}^5A$) ground state, respectively. The nature of the chemical bonding in these molecules were investigated by employing topological methods including electron localization function (ELF), atoms in molecules (AIM) as well as natural bond orbital analysis (NBO). AIM analysis suggested that the Np=N and Pu=N bonds have a covalent character. NBO results showed that these actinide complexes possess relatively strong Np=N and Pu=N bonds between the Np (Pu) *6d-5f* hybrid orbitals with N *2s-2p* orbitals. The charge decomposition analysis (CDA) diagram demonstrated that the transition of electrons mainly happened inside the AnH_2 of $HN=AnH_2$. Total and partial density of state (TDOS and PDOS) and also overlap population density of state (OPDOS) diagrams analysis were implemented. The OPDOS diagrams showed interactions for Np (Pu) and N atom have bonding character near HOMO, but have anti-bonding character at the energy region which is much lower than the HOMO. We hope that the results of this study will help researchers toward synthesis of new actinide imine materials.

Acknowledgments We are very grateful to Dr. Sobereva for many helpful discussions and providing us with the Multiwfn package. Computer time made available by the Center of High Performance Computing at Physics discipline of Sichuan University is gratefully acknowledged.

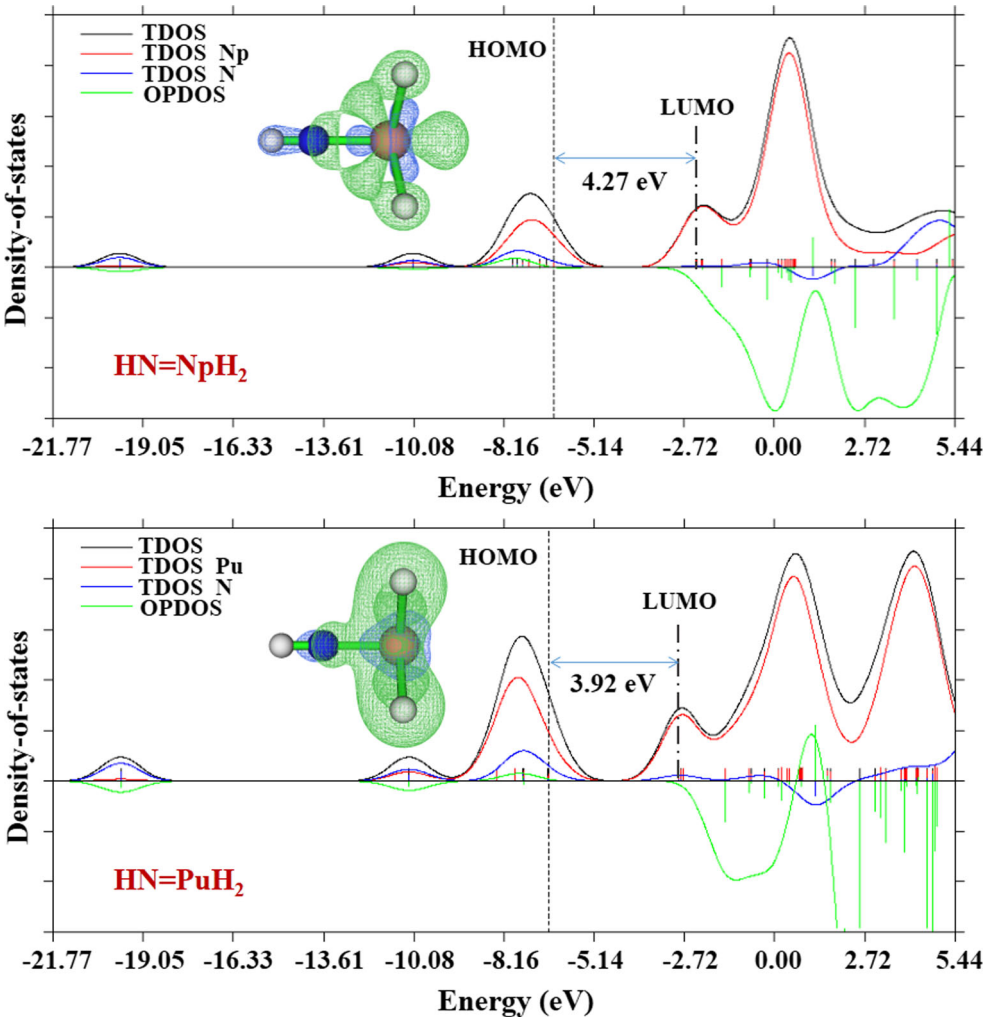

Fig. 6 The TDOS, PDOS, and OPDOS curves of $HN=NpH_2$ and $HN=PuH_2$ at the B3PW91/SDD levels of theory

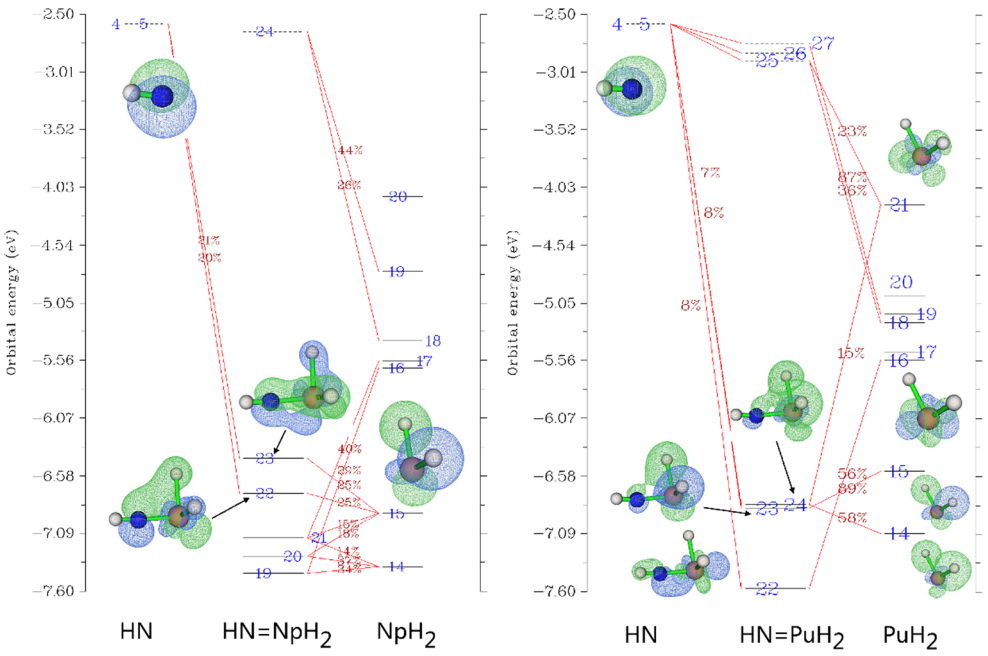

Fig. 7 Orbital-interaction diagram of $HN=NpH_2$ and $HN=PuH_2$

References

1. Brennan JG, Andersen RA (1985) J Am Chem Soc 107:514–516
2. Stevens RC, Bau R, Cramer RE, Afzal D, Gilje JW, Koetzle TF (1990) Organometallics 9:694–697
3. Gagliardi L, Pyykkö P (2004) Angew Chem Int Ed 43:1573–1576
4. Pyykkö P, Riedel S, Patzschke M (2005) Chem Eur J 11:3511–3520
5. Burns CJ (2005) Science 309:1823–1824
6. Evans WJ, Kozimor SA, Ziller JW (2005) Science 309:1835–1838
7. Hayton TW, Boncella JM, Scott BL, Palmer PD, Batista ER, Hay PJ (2005) Science 310:1941–1943
8. Hayton TW, Boncella JM, Scott BL, Batista ER, Hay PJ (2006) J Am Chem Soc 128:10549–10559
9. Frenking G, Tonner R (2007) Nature 446:276–277
10. Lyon JT, Hu HS, Andrews L, Li J (2007) PNAS 104:18919–18924
11. Graves CR, Yang P, Kozimor SA, Vaughn AE, Clark DL, Conradson SD, Schelter EJ, Scott BL, Thompson JD, Hay PJ, Morris DE, Kiplinger JL (2008) J Am Chem Soc 130:5272–5285
12. Cantat T, Arliguie T, Noel A, Thuery P, Ephritikhine M, Le Floch P, Mezailles N (2009) J Am Chem Soc 131:963–972
13. Thomson RK, Cantat T, Scott BL, Morris DL, Batista ER, Kiplinger JL (2010) Nat Chem 2:723–729
14. Fox AR, Arnold PL, Cummins CC (2010) J Am Chem Soc 132: 3250–3251
15. Wang XF, Andrews L, Vlaisavljevich B, Gagliardi L (2011) Inorg Chem 50:3826–3831
16. King DM, Tuna F, McInnes EL, McMaster J, Lewis W, Blake AJ, Liddle ST (2013) Nat Chem 5:482–488
17. Fox AR, Bart SC, Meyer K, Cummins CC (2008) Nature 455: 341–349
18. Wang XF, Andrews L, Marsden CJ (2007) Chem Eur J 13: 5601–5606
19. Wang XF, Andrews L, Marsden CJ (2008) Chem Eur J 14: 9192–9201
20. Li P, Niu WX, Gao T (2014) RSC Adv 4:29806–29817
21. Lee C, Yang W, Parr RG (1988) Phys Rev B 37:785–789
22. Becke AD (1993) J Chem Phys 98:5648–5652
23. Perdew JP, Burke K, Wang Y (1996) Phys Rev B 54:16533–16539
24. Becke AD (1998) Phys Rev A 38:3098–3100
25. Adamo C, Barone V (1999) J Chem Phys 110:6158–6170
26. Kuchle W, Dolg M, Stoll H, Preuss H (1994) J Chem Phys 100: 7535–7542
27. Frisch MJ, Trucks GW, Schlegel HB, Scuseria GE, Robb MA, Cheeseman JR, Montgomery JA Jr, Vreven T, Kudin KN et al. (2004) Gaussian 03, revision E.01. Gaussian, Inc, Wallingford
28. Michelini MC, Russo N, Sicilia E (2006) Angew Chem Int Ed 45: 1095–1099
29. Alikhani ME, Michelini MC, Russo N, Silvi B (2008) J Phys Chem A 112:12966–12974
30. Zhou J, Schlegel HB (2010) J Phys Chem A 114:8613–8617
31. Li P, Niu WX, Gao T, Wang HY (2014) Int J Quantum Chem 114: 760–768
32. De Almeida KJ, Duarte HA (2010) Organometallics 29:3735–3745
33. Lu T, Chen F (2012) J Comput Chem 33:580–592
34. Becke AD, Edgecombe KE (1990) J Chem Phys 92:5397–5403
35. Savin A, Nesper R, Wengert S, Fassler TR (1997) Angew Chem Int Ed Engl 36:1808–1832
36. Bader RFW (1990) Atoms in molecules. A quantum theory. Clarendon, Oxford
37. Hoffmann R (1988) Solids and surfaces: a chemist's view of bonding in extended structures. VCH, New York
38. Malecki JG (2010) Polyhedron 29:1973–1979
39. Dapprich S, Frenking G (1995) J Phys Chem 99:9352–9362
40. Sousa SF, Fernandes PA, Ramos MJ (2007) J Phys Chem A 111: 10439–10452
41. Bakken V, Millam JM, Schlegel HB (1999) J Chem Phys 111: 8773–8777
42. Michelini MC, Russo N, Sicilis E (2007) J Am Chem Soc 129: 4229–4239
43. Di Santo E, Michelini MC, Russo N (2009) Organometallics 28: 3716–3726
44. Palusiak M, Krygowski TM (2007) Chem Eur J 13:7996–8006
45. Farrugia LJ, Senn HM (2010) J Phys Chem A 114:13418–13433
46. De Almeida KJ, Ramalho TC, Neto JL, Santiago RT, Felicíssimo VC, Duarte HA (2013) Organometallics 32:989–999
47. Cremer D, Kraka E (1984) Angew Chem Int Ed Engl 23:627–628
48. Du J, Sun X, Chen J, Zhang L, Jiang G (2014) Dalton Trans 43: 5574–5579
49. Vyboishchikov SF, Sierraalta A, Frenking G (1996) J Comput Chem 18:416–429
50. Weinhold F, NBO 5.0 Program Manual